

dHCP Data Release 2019

Introduction

The structure of data directory and convention of files naming will follow the [BIDS specification](#) (v1.0.2) and the [organization of previous data release](#) of 40 subjects.

How to download

Via Bittorrent or download of single tar.zip file

These downloads include the outputs of processing pipelines as well as the raw images as originally acquired and reconstructed. See [Download instructions](#).

Via dHCP XNAT web service

Image data for individual subjects (without any pipeline pre-processing) can be downloaded directly through dHCP XNAT web interface. The image data are NIFTI files and if downloaded directly from the XNAT web page they will be delivered as zips. On the XNAT web interface the files are organized in the subfolders:

- <sesid>_0: anat T1 weighted image
- <sesid>_1: anat T2 weighted image
- <sesid>_2: dwi Multi-band dMRI EPI
- <sesid>_3: func Dual echo-time field-map (magnitude)
- <sesid>_4: func Dual echo-time field-map (phase difference)
- <sesid>_5: func Multi-band resting state fMRI EPI
- <sesid>_6: func Single-band reference spin echo EPI image
- <sesid>_7: func Single band reference spin echo EPI with different phase encode directions.

Support

We are supporting this data release via the `developing-hcp` tag on [neurostars](#).

Subjects

Infants were recruited and imaged at the Evelina Newborn Imaging Centre, St Thomas' Hospital, London, UK. The study was approved by the UK Health Research Authority (Research Ethics Committee reference number: 14/LO/1169) and written parental consent was obtained in every case for imaging and data release. The images included in this release were obtained from infants born and imaged between

24-45 weeks of age. The images have been reviewed for evidence of anomalies and abnormalities and a radiology score is provided, although users should verify that data they use are fit for their purposes.

Overview of data

The data release contains structural (T1w and T2w) resting state functional and diffusion images supplied as original image data and after preprocessing pipelines as described below have been applied. The neonatal brain has different tissue properties to adult brain, most strikingly it has a higher water content and myelination of white matter is incomplete. In consequences the relaxation times T1 and T2 are longer than in adult brain and white matter has longer T1 and T2 than grey matter. In neonates, brain anatomy is revealed more clearly in T2w than T1w images and thus the former are treated as the primary data for anatomical segmentation and to provide the anatomical substrates needed for functional and diffusion analysis. All neonates (with 6 exceptions) were imaged in natural sleep. If the baby woke up scanning was halted and attempts made to re-settle the subject without taking them out of the patient immobilization system. Even when sleeping peacefully, many babies move and so all data were motion corrected, mostly using methods developed specifically for the dHCP project. As a result of the challenges of imaging unsedated infants we were not able to obtain high quality and complete data for every modality on every subject. There were 558 sessions from 505 subjects with T2w images that passed QC, then of those, 512 had fMRI data that passed QC and 490 had dMRI data that passed QC. The T1w images were not subject to the same level of systematic QC as they were not processed by pre-processing pipelines. Because of their lower anatomical importance, the T1w images were placed at the end of the protocol and are of more variable quality than the T2w data.

There is a spread of gestational ages with 378 subjects in the term equivalent age range, which we defined as 37 to 44 gestational weeks. Also although these subjects were recruited as “normal subjects” (with clearly specified inclusion and exclusion criteria), there were inevitably incidental findings on the images obtained. All the anatomical images were reviewed by an expert perinatal neuroradiologist who scored the subjects using a 5 point scale (see below) - this information is provided

Acquisition details

Imaging was carried out on 3T Philips Achieva (running modified R3.2.2 software) using a dedicated neonatal imaging system which included a neonatal 32 channel phased array head coil¹. Infants were imaged without sedation except for 6 who are indicated. Anatomical images (T1w and T2w), resting state functional (rs-fMRI) and

diffusion (dMRI) acquisitions were acquired in a total examination time of 63 minutes. Sequence parameters were as follows:

Calibration scans: B0 mapping was performed using an interleaved dual TE spoiled gradient echo sequence and localised image based shimming performed for use with all EPI sequences as described in². B₀ field maps using the optimised higher order shims were subsequently re-acquired between the fMRI and dMRI acquisitions.

Anatomical acquisition: T2w and inversion recovery T1w multi-slice fast spin-echo images were each acquired in sagittal and axial slice stacks with in-plane resolution 0.8x0.8mm² and 1.6mm slices overlapped by 0.8mm (except in T1w Sagittal which used a slice overlap of 0.74mm). Other parameters were – T2w: 12000/156ms TR/TE, SENSE factor 2.11 (axial) and 2.60 (sagittal); T1w: 4795/1740/8.7ms TR/TI/TE, SENSE factor 2.27 (axial) and 2.66 (sagittal).

rs-fMRI: High temporal resolution fMRI developed for neonates³ used multiband (MB) 9x accelerated echo-planar imaging and was collected for 15 minutes, TE/TR=38/392ms gave 2300 volumes, with an acquired resolution of 2.15mm isotropic. No in-plane acceleration or partial Fourier was used. Single-band reference scans were also acquired with bandwidth matched readout, along with additional spin-echo acquisitions with both AP/PA fold-over encoding directions.

dMRI: A spherically optimized set of directions on 4 shells (b0: 20, b400: 64, b1000: 88, b2600: 128)⁴ was split into 4 optimal subsets (one per Phase Encoding Direction). These directions were then spread temporally taking motion and duty cycle considerations into account. If the baby woke up during the diffusion scan, the acquisition could be halted and restarted (after resettling the subject) with a user defined overlap in acquired diffusion weightings⁵. Acceleration of MB 4, SENSE factor 1.2 and Partial Fourier 0.86 was used, acquired resolution 1.5x1.5mm, 3mm slices with 1.5mm overlap, 3800/90ms TR/TE.

References:

1. Hughes, E. J., Winchman, T., Padormo, F., Teixeira, R., Wurie, J., Sharma, M., Fox, M., Hutter, J., Cordero-Grande, L., Price, A. N., Allsop, J., Bueno-Conde, J., Tusor, N., Arichi, T., Edwards, A. D., Rutherford, M. A., Counsell, S. J., and Hajnal J. V. A dedicated neonatal brain imaging system. *Magnetic Resonance in Medicine* (2017), 78: 794-804. DOI: [10.1002/mrm.26462](https://doi.org/10.1002/mrm.26462)
2. Gaspar, A. [Improving foetal and neonatal echo-planar imaging with image-based shimming](#). Master Thesis (2015), Universidade de Lisboa.
3. Price, A.N., Cordero-Grande, L., Malik, S.J., Abaei, M., Arichi, T., Hughes, E., Rueckert, D., Edwards, A.D., Hajnal, J.V. [Accelerated neonatal fMRI using multiband EPI](#). *ISMRM 2015*: 3911.

4. Tournier, J.D., Hughes, E., Turso, N., Sotiropoulos, N. S., Jbabdi, S., Andersson, J., Reuckert, D., Edwards, A. D., Hajnal, J. V. [Data-driven optimisation of multi-shell HARDI](#). *ISMRM 2015*: 2897.
5. Hutter, J., Tournier J. D., Price, A. N., Cordero-Grande, L., Hughes, E. J., Malik, S., Steinweg, J., Bastiani, M., Sotiropoulos, S. N., Jbabdi, S., Andersson, J., Edwards, A. D., and Hajnal, J. V. [Time-efficient and flexible design of optimised multi-shell HARDI diffusion](#). *Magnetic Resonance in Medicine* (2018), 79: 1276-1292 .

Quality Control/Assurance (QC)

QC is performed at five stages of the dHCP analysis as listed below. The final selection of subject data to release made use of these as outlined subsequently.

Five stages of QC:

- I. Scanning notes were recorded by the radiographers, and failed scans were manually flagged as pass/fail depending on if the issue affects the fMRI, the dMRI, or other.
- II. After reconstruction the images were visually inspected and each image was flagged as PASS/FAIL
- III. The structural pipeline QC combined several sources of information: 479 scans were scored visually as part of an atlas construction project -- we excluded scans with more than minor motion artifacts in T2. We excluded 11 scans we knew to be in error. We excluded scans on which the structural pipeline failed to run, or on which the separate structural QC pipeline failed to run. We did a visual inspection of all white matter surfaces and excluded one scan that was obviously failing.
- IV. The fMRI pipeline generates a number of QC metrics which are described in “Functional Pipeline” section below.
- V. The dMRI pipeline generates a number of QC metrics which are described in the “Diffusion Pipeline” section below

The inclusion criteria for fMRI data is:

- I. Must PASS fMRI scan notes QC
- II. fMRI and T2w must PASS recon QC (T1w need not pass)
- III. Must PASS structural pipeline QC
- IV. Must PASS fMRI pipeline QC

The inclusion criteria for dMRI data is:

- I. Must PASS dMRI scan notes QC
- II. dMRI and T2w must PASS recon QC (T1w need not pass)
- III. Must PASS structural pipeline QC
- IV. Must PASS dMRI pipeline QC

Pipelines

Reconstruction pipeline

The reconstruction pipeline was developed by the team at King's College London. It performs motion correction and reconstruction of T1 and T2 weighted images.

The reconstruction pipeline performs motion corrected volumetric reconstructions of multi-slice T1 and T2 weighted images extending the aligned sensitivity encoding (SENSE) method¹ to the multi-slice case². Corrections are performed for both within-plane and through-plane motion from partial k-space information. Methods and example data are available at <https://github.com/mriphysics/multiSliceAlignedSENSE/releases/tag/1.0.1>. The two acquired orthogonal stacks are integrated by a super-resolution scheme³. fMRI and dMRI simultaneous multi-slice (SMS) echo planar imaging (EPI) is reconstructed using the extended SENSE technique⁴, with details in^{5,6,7}; sensitivity estimates from a conventional reference scan are refined with the information from non-SMS reference acquisitions with matched readouts to promote matched coil map and image distortions. Sensitivity estimation uses a variational formulation⁸.

References:

1. Cordero-Grande, L., Teixeira, R. P. A. G., Hughes, E. J., Hutter, J., Price, A. N., and Hajnal, J. V. **Sensitivity encoding for aligned multishot magnetic resonance reconstruction**. *IEEE Transactions on Computational Imaging* (2016), 2(3): 266-280. DOI: [10.1109/TCI.2016.2557069](https://doi.org/10.1109/TCI.2016.2557069)
2. Cordero-Grande, L., Hughes, E. J., Hutter, J., Hutter, J., Price, A. N., and Hajnal, J. V. **Three-Dimensional Motion Corrected Sensitivity Encoding Reconstruction for Multi-Shot Multi-Slice MRI: Application to Neonatal Brain Imaging**. *Magnetic Resonance in Medicine* 2018, 79(3): 1365-1376. DOI: [10.1002/mrm.26796](https://doi.org/10.1002/mrm.26796)
3. Kuklikova-Murgasova, M., Quaghebeur, G., Rutherford, M. A., Hajnal, J. V., and Schnabel, J. A. **Reconstruction of fetal brain MRI with intensity matching and complete outlier removal**. *Medical Image Analysis* (2012), 16(8): 1550-1564. DOI: [10.1016/j.media.2012.07.004](https://doi.org/10.1016/j.media.2012.07.004)
4. Zhu, K., Dougherty, R. F., Wu, H., Middione, M. J., Takahashi, A. M, Zhang, T., Pauly, J. M., Kerr, A. B. **Hybrid-space SENSE reconstruction for simultaneous multi-slice MRI**. *IEEE Transactions on Medical Imaging*, 35(8) (2016):1824-1836. DOI: [10.1109/TMI.2016.2531635](https://doi.org/10.1109/TMI.2016.2531635)
5. Cordero-Grande, L., Price, A. N., and Hajnal, J. V. [Comprehensive CG-SENSE reconstruction of SMS-EPI](#). *ISMRM 2016*: 3239.
6. Cordero-Grande, L., Hutter, J., Price, A., Hughes, E., and Hajnal, J. V. [Goodness of fit factor in SENSE reconstruction: a tool for pseudolesion detection and fat unfolding](#). *ESMRMB 2016*: 458.

7. Hennel, F., Buehrer, M., von Deuster, C., Seuven, A., and Pruessmann, K. P. **SENSE reconstruction for multiband EPI including slice-dependent N/2 ghost correction.** *Magnetic Resonance in Medicine* (2016), 76(3): 873-879. DOI: [10.1002/mrm.25915](https://doi.org/10.1002/mrm.25915)
8. Allison, M. J., Ramani, S., and Fessler, J. A. **Accelerated regularized estimation of MR coil sensitivities using augmented Lagrangian methods.** *IEEE Transactions on Medical Imaging* (2013), 32(3): 556-564. DOI: [10.1109/TMI.2012.2229711](https://doi.org/10.1109/TMI.2012.2229711)

Structural pipeline

The structural pipeline (<https://github.com/BioMedIA/dhcp-structural-pipeline>) was encapsulated as a Docker container image and run via the OpenMOLE¹⁰ platform on a local cluster.

- I. Registration
- II. Segmentation
 - A. Structural scans are pre-processed by first running bias correction using the N4 algorithm¹.
 - B. Scans are then brain extracted using BET² from FSL.
 - C. Segmentation of the T2w volume is performed using the DRAW-EM algorithm³. DRAW-EM is an atlas-based segmentation technique that segments the volumes into 87 regions (see region names). Manually labelled atlases, annotated by an expert neuroanatomist⁴, are registered to the volume and their labels are fused to the subject space to provide structure priors. Segmentation is then performed with an Expectation-Maximization scheme that combines the structure priors and an intensity model of the volume. The 87 regions are further merged to provide the tissue segmentation (see tissue types).
 - D. All T1 weighted images have been pre-aligned to the T2w volumes using rigid alignment.
 - E. Both T1w and T2w volumes are defaced for anonymization based on registration and transformation of a manually annotated face mask.
- III. Surface extraction
 - F. Surface mesh extraction is performed with the method described in⁵. A white matter mask enclosing the white surface is computed by merging the white matter and the subcortical structures with the exception of the brainstem and the cerebellum. Similarly, a pial mask is computed by merging the grey matter structure with the white matter mask. The white and pial surfaces of the left and right hemispheres are then reconstructed with the method outlined in⁵ using a deformable model. The model in⁵ includes forces to avoid self-intersections and includes an image-based refinement step that corrects regions such as deep sulci mislabelled by the volumetric segmentation.

- G. Midthickness surfaces are generated as the middle surface between the white and pial surfaces. The midthickness surface is computed using the Euclidean distance between corresponding points of the white and pial surface.
- H. Spherical projection is performed⁶, and it is based on the inflated white matter surface. The inflated white matter surface is produced in a similar manner as in the FreeSurfer pipeline⁷. Inflated and very inflated surfaces used for visualisation are generated similarly to⁸.
- I. The following metrics are further estimated from the surfaces: curvature, thickness, sulcal depth, T1w/T2w myelin, labels (projected from the volume). All surfaces have one-to-one vertex correspondence for all points on the surface ensuring that the same vertex indexes the same point, in the same relative position, on the anatomy for all surfaces.
The structural pipeline is described in detail⁹.

References:

1. Tustison, N. J., Avants, B. B., Cook, P. A., Zheng, Y., Egan, A., Yushkevich, P. A. and Gee, J. C. **N4ITK: improved N3 bias correction**. *IEEE transactions on medical imaging (2010)*, 29(6): 1310-1320. DOI: [10.1109/TMI.2010.2046908](https://doi.org/10.1109/TMI.2010.2046908)
2. Smith, S. M. **Fast robust automated brain extraction**. *Human Brain Mapping (2002)*, 17(3): 143-55. DOI: [10.1002/hbm.10062](https://doi.org/10.1002/hbm.10062)
3. Makropoulos, A., Gousias I. S., Ledig C., Aljabar P., Serag A, Hajnal J. V., Edwards A. D., Counsell S. J., and Rueckert D. **Automatic whole brain MRI segmentation of the developing neonatal brain**. *IEEE transactions on medical imaging (2014)*, 33(9): 1818-1831. DOI: [10.1109/TMI.2014.2322280](https://doi.org/10.1109/TMI.2014.2322280)
4. Gousias, I. S., Edwards A. D., Rutherford M. A., Counsell S. J., Hajnal J. V., Rueckert D., and Hammers, A. **Magnetic resonance imaging of the newborn brain: manual segmentation of labelled atlases in term-born and preterm infants**. *Neuroimage (2012)*, 62(3): 1499-1509. DOI: [10.1016/j.neuroimage.2012.05.083](https://doi.org/10.1016/j.neuroimage.2012.05.083)
5. Schuh, A., Makropoulos, A., Wright, R., Robinson, E. C., Tusor, N., Steinweg, J., Hughes, E., Cordero Grande, L., Price, A., Hutter, J., Hajnal, J., and Rueckert, D. **A deformable model for reconstruction of the neonatal cortex**. *IEEE 14th International Symposium on Biomedical Imaging 2017*. DOI: [10.1109/ISBI.2017.7950639](https://doi.org/10.1109/ISBI.2017.7950639)
6. Elad, A., Keller, Y., and Kimmel, R. [Texture Mapping via Spherical Multidimensional Scaling](#). *International Conference on Scale-Space Theories in Computer Vision (2005)*: 443–455.
7. Fischl, B., Sereno M. I., and Dale, A. M. **Cortical surface-based analysis: II: inflation, flattening, and a surface-based coordinate system**. *Neuroimage (1999)*, 9(2): 195-207. DOI: [10.1006/nimg.1998.0396](https://doi.org/10.1006/nimg.1998.0396)
8. Glasser, M., Sotiropoulo, S. N., Wilson, J. A, Coalson, T. S, Fischl, B., Andersson, L., Xu, J., Jbabdi, S., Webster, M., Polimeni, J. R., Van Essen, D. C., Jenkinson, M., WU-Minn HCP Consortium. **The minimal preprocessing pipelines for the Human**

Connectome Project. *NeuroImage* (2013), 80: 105–124. DOI: [10.1016/j.neuroimage.2013.04.127](https://doi.org/10.1016/j.neuroimage.2013.04.127)

9. Makropoulos, A., Robinson, E., Schuh, A., Wright, R., Fitzgibbon, S., Bozek, J., Counsell, S. J., Steinweg, J., Vecchiato, K., Passerat-Palmbach, J., Lenz, G., Mortari, F., Tenev, T., Duff, E. P., Bastiani, M., Cordero-Grande, L., Hughes, E., Tusor, N., Tournier, J. D., Hutter, J., Price, A. N., Teixeira, R. P. A. G., Murgasova M, Victor, S., Kelly, C., Rutherford, M. A., Smith, S. M., Edwards, A. D., Hajnal, J. V., Jenkinson, M., and Rueckert, D. **The developing Human Connectome Project: a Minimal Processing Pipeline for Neonatal Cortical Surface Reconstruction.** *NeuroImage* (2018), 173: 88-112. DOI: [10.1016/j.neuroimage.2018.01.054](https://doi.org/10.1016/j.neuroimage.2018.01.054)
10. Passerat-Palmbach, J., Reuillon, R., Leclaire, M., Makropoulos, A., Robinson, E.C., Parisot, S., and Rueckert, D. **Reproducible Large-Scale Neuroimaging Studies with the OpenMOLE Workflow Management System.** *Frontiers in Neuroinformatics* (2017), 11. DOI: [10.3389/fninf.2017.00021](https://doi.org/10.3389/fninf.2017.00021)

Diffusion pipeline

For a complete and detailed description of all the steps involved in the dHCP neonatal diffusion MRI (dMRI) data processing pipeline (https://git.fmrib.ox.ac.uk/matteob/dHCP_neo_dMRI_pipeline_release), the reader is referred to¹. The main processing steps are briefly summarised below:

- I. For each phase encoding (PE) direction, the diffusion un-weighted b0 volume pairs least-affected by intra-volume motion are automatically selected. The dataset is then re-organised by moving the least-affected b0 volume and the volumes that follow (until the end of the acquisition) at the beginning of the 4D raw data file.
- II. Field maps for correcting susceptibility-induced distortions are estimated using FSL TOPUP².
- III. Distortions caused by susceptibility, motion, motion-induced signal drop-out and eddy currents are corrected; outlier slices are detected and replaced in raw distorted space using FSL EDDY³⁻⁶.
- IV. A super-resolution algorithm⁷ is applied along the slice-selection direction, to achieve isotropic resolution of 1.5 mm.
- V. Diffusion data are aligned to high-resolution structural (T2-weighted) space using boundary-based registration^{8, 9} on the average attenuation volume for the b=1000 s/mm² shell (i.e. b1k/b0). This transformation is combined with a non-linear registration¹⁰ of the T2w volume to the 40 weeks template¹¹ to allow transformations between diffusion and atlas spaces.

Diffusion MRI QC

- I. Numerous quality assurance metrics are calculated by the EDDY QC tools¹². Four of these are specifically compared against the population distribution to flag outliers for manual inspection and potential exclusion:
 - A. Mean signal-to-noise ratio (SNR) from the b0 volumes

- B. Mean contrast-to-noise ratio (CNR) for each b-shell, i.e., 400, 1000 and 2600 s/mm².
- II. All QC metrics are then converted to Z-scores and averaged, to generate a summary QC metric. Subject/sessions with a summary Z-score < -2.0 were excluded.

References:

1. Bastiani, M., Andersson, J.L.R., Cordero-Grande, L., Murgasova, M., Hutter, J., Price, A.N., Makropoulos, A., Fitzgibbon, S.P., Hughes, E., Rueckert, D., Victor, S., Rutherford, M., Edwards, A.D., Smith, S.M., Tournier, J.D., Hajnal, J.V., Jbabdi, S., and Sotiropoulos, S.N. **Automated processing pipeline for neonatal diffusion MRI in the developing Human Connectome Project.** *Neuroimage* (2019), 185: 750-763. DOI: [10.1016/j.neuroimage.2018.05.064](https://doi.org/10.1016/j.neuroimage.2018.05.064)
2. Andersson, J.L., Skare, S., and Ashburner, J. **How to correct susceptibility distortions in spin-echo echo-planar images: application to diffusion tensor imaging.** *Neuroimage* (2003), 20(2): 870-888. DOI: [10.1016/S1053-8119\(03\)00336-7](https://doi.org/10.1016/S1053-8119(03)00336-7)
3. Andersson, J.L., and Sotiropoulos, S.N. **An integrated approach to correction for off-resonance effects and subject movement in diffusion MR imaging.** *Neuroimage* (2016), 125: 1063-1078. DOI: [10.1016/j.neuroimage.2015.10.019](https://doi.org/10.1016/j.neuroimage.2015.10.019)
4. Andersson, J.L.R., Graham, M.S., Drobnyak, I., Zhang, H., and Campbell, J. **Susceptibility-induced distortion that varies due to motion: Correction in diffusion MR without acquiring additional data.** *NeuroImage* (2018), 171: 277-295. DOI: [10.1016/j.neuroimage.2017.12.040](https://doi.org/10.1016/j.neuroimage.2017.12.040)
5. Andersson, J.L.R., Graham, M.S., Drobnyak, I., Zhang, H., Filippini, N., and Bastiani, M. **Towards a comprehensive framework for movement and distortion correction of diffusion MR images: Within volume movement.** *Neuroimage* (2017), 152: 450-466. DOI: [10.1016/j.neuroimage.2017.02.085](https://doi.org/10.1016/j.neuroimage.2017.02.085)
6. Andersson, J.L.R., Graham, M.S., Zsoldos, E., and Sotiropoulos, S.N. **Incorporating outlier detection and replacement into a non-parametric framework for movement and distortion correction of diffusion MR images.** *Neuroimage* (2016), 141: 556-572. DOI: [10.1016/j.neuroimage.2016.06.058](https://doi.org/10.1016/j.neuroimage.2016.06.058)
7. Kuklisova-Murgasova, M., Quaghebeur, G., Rutherford, M.A., Hajnal, J.V., and Schnabel, J.A. **Reconstruction of fetal brain MRI with intensity matching and complete outlier removal.** *Med Image Anal* (2012), 16(8): 1550-1564. DOI: [10.1016/j.media.2012.07.004](https://doi.org/10.1016/j.media.2012.07.004)
8. Greve, D.N., and Fischl, B. **Accurate and robust brain image alignment using boundary-based registration.** *Neuroimage* (2009), 48(1): 63-72. DOI: [10.1016/j.neuroimage.2009.06.060](https://doi.org/10.1016/j.neuroimage.2009.06.060)
9. Jenkinson, M., Bannister, P., Brady, M., and Smith, S. **Improved optimization for the robust and accurate linear registration and motion correction of brain image.** *Neuroimage* (2002), 17(2): 825-841. DOI: [10.1006/nimg.2002.1132](https://doi.org/10.1006/nimg.2002.1132)
10. Andersson, J.L.R., Jenkinson, M., and Smith, S. [Non-linear registration. aka spatial normalisation.](#) *FMRIB technical report TR07JA2* (2010).

11. Schuh, A., Makropoulos, A., Robinson, E.C., Cordero-Grande, L., Hughes, E., Hutter, J., Price, A.N., Murgasova, M., Teixeira, R.P.A.G., Tusor, N., Steinweg, J.K., Victor, S., Rutherford, M.A., Hajnal, J.V., Edwards, A.D., and Rueckert, D. **Unbiased construction of a temporally consistent morphological atlas of neonatal brain development.** *bioRxiv* (2018), 251512. DOI: [10.1101/251512](https://doi.org/10.1101/251512)
12. Bastiani, M., Cottaar, M., Fitzgibbon, S.P., Suri, S., Alfaro-Almagro, F., Sotiropoulos, S.N., Jbabdi, S., and Andersson, J.L.R. **Automated quality control for within and between studies diffusion MRI data using a non-parametric framework for movement and distortion correction.** *Neuroimage* (2019), 184: 801-812. DOI: [10.1016/j.neuroimage.2018.09.073](https://doi.org/10.1016/j.neuroimage.2018.09.073)

Functional pipeline

Pre-processing for fMRI:

- I. Prepare fieldmaps for correction of susceptibility distortions
 - A. Estimate field map from the two “best” spin-echo volumes (1 per phase-encode direction) using FSL TOPUP¹
 1. “Best” is defined by smoothness in the z-dimension (stdev of the slice-to-slice difference in the z-dimension)
 - B. If visual inspection indicates that the spin-echo has significant motion contamination then use the dual-echo-derived fieldmap instead of the spin-echo-derived fieldmap
- II. Registration:
 - A. Boundary-based registration (BBR, FSL FLIRT³) of the fieldmap to the T2 structural
 - B. Boundary-based registration (BBR, FSL FLIRT³) of the sbref to the T2 structural incorporating field map-based distortion correction of the sbref
 - C. Linear registration (6-dof, corratio, FSL FLIRT³) of the first volume of the functional multiband EPI to the sbref
 - D. After susceptibility and motion correction, linear registration (6-dof, corratio, FSL FLIRT³) of the temporal mean of the motion and distortion corrected functional multiband EPI to the distortion corrected sbref
 - E. Nonlinear diffeomorphic multimodal registration of the age-matched T1/T2 templates from the dHCP volumetric atlas (Schuh et al., 2018) to the subjects T1/T2 structurals using ANTs SyN (Avants, Epstein, Grossman, & Gee, 2008). If the age of the subject is outside the range covered by the atlas (36-43) then it is registered to the closest template age within the atlas. We have augmented the dHCP volumetric atlas with week-to-week nonlinear transforms estimated using a diffeomorphic multi-modal (T1/T2) registration (ANTs SyN). The appropriate transforms are then combined to yield a (40 week) template-to-structural transform
 - F. From these primary registrations the following composite transforms are calculated:

- i. fieldmap to native functional
 - li. motion and distortion corrected functional to 40-week template from the dHCP volumetric atlas
- III. Susceptibility and motion correction
 - A. Slice-to-volume motion correction and motion-by-susceptibility correction is performed using FSL EDDY²
- IV. ICA Denoising
 - A. Temporal high-pass filter (150s high-pass cutoff) and ICA denoising using FSL FIX⁴, pre-trained with manually-labelled data from 35 dHCP neonatal subjects, to identify artefactual ICs (accuracy: median TPR=100%, median TNR=95.4%). The ICA dimensionality was capped at 600 ICs.
 - B. Noise ICs and motion parameters regressed from motion and distortion corrected functional multiband EPI.

fMRI QC:

- I. Numerous quality assurance metrics are calculated during the pre-processing. Six of these are specifically compared against the population distribution to flag outliers for manual inspection and potential exclusion:
 - A. Mean DVARS⁵ of the ICA denoised functional EPI
 - B. Mean tSNR of the ICA denoised functional EPI
 - C. Normalised mutual information of the source (moving) image, re-sampled to reference space, and the reference (fixed) image, for each of the primary registrations:
 - 1. Fieldmap to structural T2
 - 2. Native functional to sbref
 - 3. Motion and distortion corrected functional to sbref
 - 4. Sbref to structural T2
 - 5. Age-matched atlas template T2 to native structural T2
- II. All QA measures were converted to Z-scores and flipped as necessary so that positive z-scores are good and negative bad. Subject/sessions with a z-score < -2.5 on any QC metric were excluded.

References:

1. Andersson, J. L., Skare, S. and Ashburner, J. **How to correct susceptibility distortions in spin-echo echo-planar images: application to diffusion tensor imaging.** *Neuroimage* (2003), 20: 870-888. DOI: [10.1016/S1053-8119\(03\)00336-7](https://doi.org/10.1016/S1053-8119(03)00336-7)
2. Andersson, J. L. and Sotiropoulos, S. N. **An integrated approach to correction for off-resonance effects and subject movement in diffusion MR imaging.** *Neuroimage* (2016), 125: 1063-1078. DOI: [10.1016/j.neuroimage.2015.10.019](https://doi.org/10.1016/j.neuroimage.2015.10.019)

3. Jenkinson, M., and Smith, S. **A global optimisation method for robust affine registration of brain images.** *Medical image analysis* (2001), 5(2): 143–156. DOI: [10.1016/S1361-8415\(01\)00036-6](https://doi.org/10.1016/S1361-8415(01)00036-6)
4. Salimi-Khorshidi, G., Douad, G, Beckman, C. F., Glasser, M. F., Griffanti, L., and Smith, S. M. **Automatic denoising of functional MRI data: combining independent component analysis and hierarchical fusion of classifiers.** *NeuroImage* (2014), 90: 449–468. DOI: [10.1016/j.neuroimage.2013.11.046](https://doi.org/10.1016/j.neuroimage.2013.11.046)
5. Power, J. D., Barnes, K. A., Snyder, A. Z., Schlaggar, B. L., and Petersen, S. E. **Spurious but Systematic Correlations in Functional Connectivity MRI Networks Arise from Subject Motion.** *NeuroImage* (2012), 59(3): 2142–54. DOI: [10.1016/j.neuroimage.2011.10.018](https://doi.org/10.1016/j.neuroimage.2011.10.018)

Metadata

The `participants.tsv` for each BIDS pipeline has a number of extra columns beyond `participant_id`. These have the following meaning:

<code>gender</code>	Male / Female
<code>birth_age</code>	Gestational age at birth in weeks
<code>birth_weight</code>	Birthweight (kg)
<code>singleton</code>	Singleton / multiple status of the pregnancy

The `sessions.tsv` file has extra columns beyond `session_id`. These have the following meaning:

<code>scan_age</code>	Gestational age at scan in weeks
<code>scan_head_circumference</code>	Head circumference (cm)
<code>scan_number</code>	1 for the first scan, 2 for the second
<code>radiology_score</code>	The MRI scans were reviewed by a specialist perinatal neuroradiologist who scored each subject using the following scale: 1=Normal appearance for age 2=Incidental findings with unlikely significance for clinical outcome or analysis (e.g. <i>subdural haemorrhage. Isolated subependymal cysts. Mild inferior vermis rotation</i>) 3=Incidental findings with unlikely clinical significance but possible analysis significance (e.g. several punctate lesions or other focal white matter / cortical lesions not thought to be of clinical significance) 4=Incidental findings with possible clinical significance. Unlikely analysis significance (e.g. Isolated non brain anomaly for example in pituitary / on tongue) 5=Incidental finding with possible / likely significance for

	both clinical and imaging analysis (e.g. Major lesions within white matter cortex, cerebellum and or basal ganglia; small head / brain < 1 st centile) Q=Poor quality anatomical data
sedation	1 if the subject was sedated during the scan, 0 otherwise

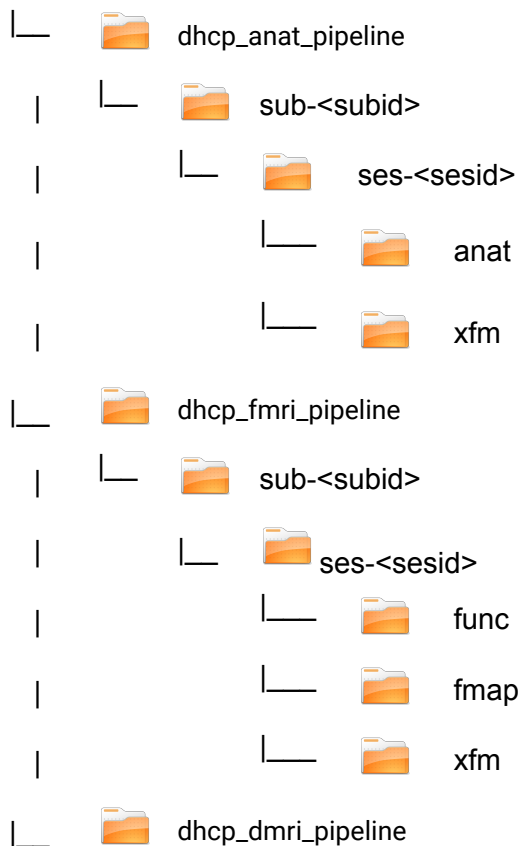
As a convenience, an extra top-level file called `combined.tsv` lists all these fields for all scans in a single large table.

Data directory structure and naming convention

The data directory structure and naming of files is organized as follows.

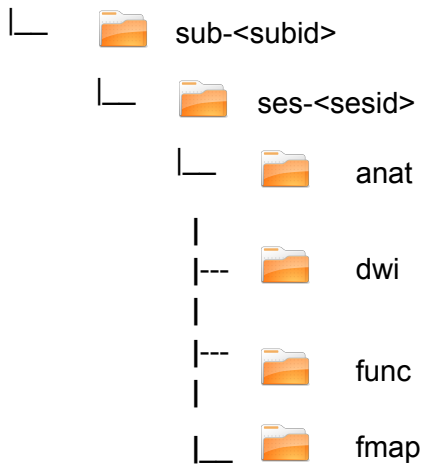
<subid>	subject ID
<sesid>	refers to session ID
CSF	cerebrospinal fluid
WM	white matter
cGM	cortical grey matter
sGM	subcortical grey matter
EPI	echo-planar imaging

derivatives (contains output files from pipelines)





 **sourcedata (contains input files for pipelines)**



Explanation of filenames

Structural pipeline

Inputs:

Reconstructed data: `sourcedata/sub-<subid>/ses-<sesid>/anat`

T1 weighted image	<code>sub-<subid>_ses-<sesid>_T1w.nii.gz</code>
T2 weighted image	<code>sub-<subid>_ses-<sesid>_T2w.nii.gz</code>

Outputs:

Derived data: `derivatives/dhcp_anat_pipeline/sub-<subid>/ses-<sesid>`

FSL BET brain mask	<code>anat/sub-<subid>_ses-<sesid>_desc-bet_space-T2w_brainmask.nii.gz</code>
Draw-EM brain mask	<code>anat/sub-<subid>_ses-<sesid>_desc-drawem_space-T2w_brainmask.nii.gz</code>
Draw-EM regional segmentation (87 labels)	<code>anat/sub-<subid>_ses-<sesid>_desc-drawem87_space-T2w_dseg.nii.gz</code>

Draw-EM tissue segmentation (9 labels)	anat/sub-<subid>_ses-<sesid>_desc-drawem9_space-T2w_dseg.nii.gz
Cortical ribbon	anat/sub-<subid>_ses-<sesid>_desc-ribbon_space-T2w_dseg.nii.gz
T1 weighted image (in T2 space)	anat/sub-<subid>_ses-<sesid>_space-T2w_T1w.nii.gz
T1 weighted, bias corrected image (in T2 space)	anat/sub-<subid>_ses-<sesid>_desc-restore_space-T2w_T1w.nii.gz
T2 weighted, bias corrected image	anat/sub-<subid>_ses-<sesid>_desc-restore_T2w.nii.gz
T1/T2 ratio	anat/sub-<subid>_ses-<sesid>_space-T2w_myelinmap.nii.gz
T1/T2 ratio on the cortical ribbon	anat/sub-<subid>_ses-<sesid>_space-T2w_desc-myelinmapribbon_dseg.nii.gz
QC report	sub-<subid>_ses-<sesid>_qc.pdf

surface files	
Left/Right white surface	anat/sub-<subid>_ses-<sesid>_hemi-{L R}_space-T2w_wm.surf.gii
Left/Right pial surface	anat/sub-<subid>_ses-<sesid>_hemi-{L R}_space-T2w_pial.surf.gii
Left/Right mid-thickness surface	anat/sub-<subid>_ses-<sesid>_hemi-{L R}_space-T2w_midthickness.surf.gii
Left/Right inflated surface	anat/sub-<subid>_ses-<sesid>_hemi-{L R}_space-T2w_inflated.surf.gii
Left/Right very inflated surface	anat/sub-<subid>_ses-<sesid>_hemi-{L R}_space-T2w_veryinflated.surf.gii
Left/Right spherical surface	anat/sub-<subid>_ses-<sesid>_hemi-{L R}_space-T2w_sphere.surf.gii
Cortical curvature	anat/sub-<subid>_ses-<sesid>_space-T2w_curv.dscalar.nii
Left/Right cortical curvature	anat/sub-<subid>_ses-<sesid>_hemi-{L R}_space-T2w_curv.shape.gii
Sulcal depth	anat/sub-<subid>_ses-<sesid>_space-T2w_sulc.dscalar.nii
Left/Right sulcal depth	anat/sub-<subid>_ses-<sesid>_hemi-{L R}_space-T2w_sulc.shape.gii
Cortical thickness	anat/sub-<subid>_ses-<sesid>_space-T2w_thickness.dscalar.nii
Left/Right cortical thickness	anat/sub-<subid>_ses-<sesid>_hemi-{L R}_space-T2w_thickness.shape.gii
Cortical thickness (curvature	anat/sub-<subid>_ses-<sesid>_desc-corr_space-T

regressed out)	<code>2w_thickness.dscalar.nii</code>
Left/Right cortical thickness (curvature regressed out)	<code>anat/sub-<subid>_ses-<sesid>_hemi-{L R}_desc-corr_space-T2w_thickness.shape.gii</code>
Cortical myelin	<code>anat/sub-<subid>_ses-<sesid>_space-T2w_myelinmap.dscalar.nii</code>
Left/Right cortical myelin	<code>anat/sub-<subid>_ses-<sesid>_hemi-{L R}_space-T2w_myelinmap.shape.gii</code>
Smoothed cortical myelin	<code>anat/sub-<subid>_ses-<sesid>_desc-smoothed_space-T2w_myelinmap.dscalar.nii</code>
Left/Right smoothed cortical myelin	<code>anat/sub-<subid>_ses-<sesid>_hemi-{L R}_desc-smoothed_space-T2w_myelinmap.shape.gii</code>
Cortical regional labels projected from volume	<code>anat/sub-<subid>_ses-<sesid>_desc-drawem_space-T2w_dparc.dlabel.nii</code>
Left/Right cortical regional labels projected from volume	<code>anat/sub-<subid>_ses-<sesid>_hemi-{L R}_desc-drawem_space-T2w_dparc.dlabel.gii</code>
Left/Right Medial wall	<code>anat/sub-<subid>_ses-<sesid>_hemi-{L R}_desc-medialwall_mask.shape.gii</code>
Workbench file for loading surfaces	<code>anat/wb.spec</code>
Folder containing registration files	<code>xfm/</code>
Warp from structural space to the subject's age respective template space	<code>xfm/sub-<subid>_ses-<sesid>_from-T2w_to-template{subage}wk_mode-image.nii.gz</code>
Warp from the subject's age respective template space to the structural space	<code>xfm/sub-<subid>_ses-<sesid>_from-template{subage}wk_to-T2w_mode-image.nii.gz</code>
Warp from structural space to the 40 weeks template space	<code>xfm/sub-<subid>_ses-<sesid>_from-T2w_to-template40wk_mode-image.nii.gz</code>
Warp from the 40 weeks template space to the structural space	<code>xfm/sub-<subid>_ses-<sesid>_from-template40wk_to-T2w_mode-image.nii.gz</code>

Diffusion pipeline

Inputs:

Reconstructed data: `sourcedata/sub-<subid>/ses-<sesid>/dwi`

Multi-band dMRI EPI	<code>sub-<subid>_ses-<sesid>_dwi.nii.gz</code>
List of b-values	<code>sub-<subid>_ses-<sesid>_dwi.bval</code>
List of gradient directions	<code>sub-<subid>_ses-<sesid>_dwi.bvec</code>

Structural pipeline derived data:

derivatives/dhcp_anat_pipeline/sub-<subid>/ses-<sesid>

T2 weighted, bias corrected and brain extracted image	sub-<subid>_ses-<sesid>_T2w.nii.gz
Draw-EM tissue segmentation (9 labels)	sub-<subid>_ses-<sesid>_space-T2w_desc-drawem_dseg.nii.gz
T2 brain mask	sub-<subid>_ses-<sesid>_space-T2w_brainmask.nii.gz

Outputs:

Derived data: derivatives/dhcp_dmri_pipeline/sub-<subid>/ses-<sesid>

Eddy current, susceptibility-by-motion and motion (within and between volumes) corrected super-resolved 4D volume with outlier rejection and replacement	dwi/sub-<subid>_ses-<sesid>_desc-preproc_dwi.nii.gz
List of b-values	dwi/sub-<subid>_ses-<sesid>_desc-preproc_dwi.bval
List of post-EDDY rotated gradient directions	dwi/sub-<subid>_ses-<sesid>_desc-preproc_dwi.bvec
Brain mask	dwi/sub-<subid>_ses-<sesid>_desc-preproc_space-dwi_brainmask.nii.gz
Estimated field map	fmap/sub-<subid>_ses-<sesid>_fieldmap.nii.gz
QC report	sub-<subid>_ses-<sesid>_qc.pdf
Rigid-body transform from structural to diffusion space	xfm/sub-<subid>_ses-<sesid>_from-T2w_to-dwi_mode-image.mat
Rigid-body transform from diffusion to structural space	xfm/sub-<subid>_ses-<sesid>_from-dwi_to-T2w_mode-image.mat
Warp from diffusion space to 40 week template space (Schuh)	xfm/sub-<subid>_ses-<sesid>_from-dwi_to-template40wk_mode-image.nii.gz
Warp from 40 week template space (Schuh) to diffusion space	xfm/sub-<subid>_ses-<sesid>_from-template40wk_to-dwi_mode-image.nii.gz

Functional pipeline

Inputs:

Reconstructed data: sourcedata/sub-<subid>/ses-<sesid>

Resting fMRI	func/sub-<subid>_ses-<sesid>_task-rest_bold.nii.gz
Single-band Ref	func/sub-<subid>_ses-<sesid>_task-rest_sbref.nii.gz
Spin Echo EPI with different phase encode directions (for topup fieldmap estimation)	fmap/sub-<subid>_ses-<sesid>-{sesid}_dir-APPA_epi.nii.gz
Dual echo-time field-map, magnitude	fmap/sub-<subid>_ses-<sesid>_magnitude.nii.gz
Dual echo-time field-map	fmap/sub-<subid>_ses-<sesid>_fieldmap.nii.gz

Structural pipeline derived data:

derivatives/dhcp_anat_pipeline/sub-<subid>/ses-<sesid>

T2 weighted, bias corrected image (in T2 space)	anat/sub-<subid>_ses-<sesid>_T2w.nii.gz
T2 brain mask	anat/sub-<subid>_ses-<sesid>_space-T2w_brainmask.nii.gz
Draw-EM tissue segmentation (9 labels)	anat/sub-<subid>_ses-<sesid>_space-T2w_desc-drawem_dseg.nii.gz
T1 weighted, bias corrected image (in T2 space)	anat/sub-<subid>_ses-<sesid>_space-T2w_T1w.nii.gz

Outputs:

Derived data: derivatives/dhcp_fmri_pipeline/sub-<subid>/ses-<sesid>

Multi-band EPI, distortion corrected, motion corrected, FIX denoised, 4D image	func/sub-<subid>_ses-<sesid>_task-rest_desc-preproc_bold.nii.gz
Motion parameters	func/sub-<subid>_ses-<sesid>_motion.tsv
Brain mask	func/sub-<subid>_ses-<sesid>_task-rest_desc-preproc_space-bold_brainmask.nii.gz
Derived fieldmap, magnitude	fmap/sub-<subid>_ses-<sesid>_magnitude.nii.gz
Derived fieldmap (rad/s)	fmap/sub-<subid>_ses-<sesid>_fieldmap.nii.gz
QC report	sub-<subid>_ses-<sesid>_funcqc.html
Folder containing registration files	xfm

Rigid-body transform from functional (mcdc) to single-band Ref space	<code>xfm/sub-<subid>_ses-<sesid>_from-bold_to-sbref_mode-image.mat</code>
Rigid-body transform from single-band Ref space to structural space	<code>xfm/sub-<subid>_ses-<sesid>_from-sbref_to-T2w_mode-image.mat</code>
Rigid-body transform from functional (mcdc) to structural space	<code>xfm/sub-<subid>_ses-<sesid>_from-bold_to-T2w_mode-image.mat</code>
Rigid-body transform from field-map to structural space	<code>xfm/sub-<subid>_ses-<sesid>_from-fieldmap_to-T2w_mode-image.mat</code>
Warp from functional (mcdc) space to the 40 weeks template space	<code>xfm/sub-<subid>_ses-<sesid>_from-bold_to-template40wk_mode-image.nii.gz</code>
Warp from the structural space to the 40wk template space	<code>xfm/sub-<subid>_ses-<sesid>_from-T2w_to-template40wk_mode-image.nii.gz</code>